Elastic constant of dielectric nano-thin films using three-layer resonance studied by picosecond ultrasonics

Hiroki Fukuda, Akira Nagakubo,* and Hirotsugu Ogi

Graduate School of Engineering, Osaka University, Suita, Osaka 565-0871, Japan

Elastic constants and sound velocities of nm-order thin films are important for acoustic filters. However, it is difficult to measure them for dielectric films. In this study, we use a three-layer structure where a dielectric nano-thin film is sandwiched between thicker metallic films to measure the longitudinal elastic constant of the dielectric film. We propose an efficiency function to estimate the optimal thicknesses of the components. We use Pt/NiO/Pt three layers for confirming our proposed method. Determined elastic constant of NiO deposited at room temperature is smaller than the bulk value by ∼40%, however, it approaches to the bulk value as the deposition temperature increases. We also reveal that uncertainty of the elastic constant of Pt does not affect that of NiO in this structure.

1. Introduction

Elastic constants and sound velocities of thin films are essential parameters of surface acoustic wave (SAW) filters[1–4] and film bulk acoustic resonators (FBAR)[5–7] for wireless communication. They are also essential parameters in an acoustic mirror, which enhances Q values of the filters.[8,9] Next-generation communication uses much higher-frequency band pass filters,[10,11] which are composed of much thinner films. For example, in our previous study, we showed that 10.9-nm NiO and 7.6-nm Pt multilayer enhanced 140-GHz resonance.[12] Therefore, it is important to measure elastic constants and sound velocities of nm-order thin films. Picosecond ultrasonics can directly excite and detect GHz–THz range ultrasound in metallic and semiconductor nm-order thin film through the laser absorption.[13,14] Using this method, we have measured the longitudinal elastic constants of 5–110 nm metallic thin films by observing through-thickness resonances or pulse echoes, and revealed that they are usually smaller than those of bulk vales by 5–30%.[15–17] This softening in thin film insists that bulk values should not be adopted in designing the acoustic filters, and the elastic constants of thin film should be measured.

However, it is significantly difficult to measure the elastic constants of a dielectric nm-order thin film, which plays an important role in the filters. SiO_2 is used as a temperature compensate material[18,19] because it has positive temperature dependence of sound velocity.[20,21] Acoustic reflectors is consists of high and low acoustic impedance materials, where dielectric thin film is used as the low-impedance material.[22,23] By depositing ∼10 nm metallic film, picosecond ultrasonics can excite ultrasound in dielectric material through the thermal expansion of the metal.[24] For "thick" nm films (420–4000 nm), we have measured the longitudinal elastic constants and sound velocities of SiO_2,[25,26] SiON,[27] and AlN[28] films by observing Brillouin oscillation.[29,30] For these films, we deposited ∼10 nm metallic films to excite an acoustic pulse. Brillouin oscillation is caused by light interference between reflected light at the surface and diffracted light by the propagating acoustic pulse in the dielectric material, and its period corresponds to the half of the wavelength of probe light in the material. However, it is difficult to accurately measure the elastic constant of dielectric thin film less than ∼100 nm because we can not determine Brillouin-oscillation frequency in a thinner film than the wavelength of probe light in it.

In this study, we propose a resonance method to measure the elastic constant of ∼30 nm dielectric thin film sandwiched by metallic thin films using picosecond ultrasonics. We deposit Pt/NiO/Pt three-layer film and excite through-thickness resonances. In this structure, the strain energy of the fundamental mode becomes larger in the NiO layer, which makes its frequency sensitive to the elastic constant of NiO (C_{NiO}). Therefore, by measuring the fundamental-mode frequency, we can determine C_{NiO} even if the elastic constant of Pt (C_{Pt}) includes uncertainty. Thinner Pt-film thickness makes the resonance frequency more insensitive to C_{Pt}, however, we need the Pt layer to excite and detect resonance. Therefore, we calculate the contribution of C_{NiO} to resonance frequencies, and propose an efficiency function by considering the contribution and excitation-detection efficiency of light to estimate the optimal Pt thickness in this structure. We prepare four structures by changing the Pt-film thickness remaining the NiO-film thickness. We observe 20–50 GHz resonances by picosecond ultrasonics, and compare the vibration amplitudes with the calculated efficiency function, determining the optimal thickness to be ∼18 nm. Thus, we make Pt/NiO/Pt films with different deposition temperatures between 300 and 700 K, and inversely determine C_{NiO}. We also make Pt single layers under the same conditions, and measure their elastic constants to evaluate the effects of them for C_{NiO} in the inverse calculation. We discuss the effects of uncertainty in C_{Pt} and the thickness of each layer, confirming the validity of this method.

2. Experimental methods

2.1 Thin films

We used three substrates in this study: (0001)-Al_2O_3 (AO), (100)-Si, and (100)-Si with thermally oxidized surface (TO-Si). They were cleaned by ultrasonication in N-Methyl-2-pyrrolidone, isopropyl alcohol, and then distilled water. Then, we further remove contamination on the surface by ambient-gas plasma cleaning for 10 min. We deposited Pt and NiO films by the RF magnetron sputtering method. Base pressure, Ar pressure, and sputtering power were $\sim 1\times10^{-5}$ Pa, 0.8 Pa, and 50 W, respectively. The thin films were deposited at three temperatures of 293, 553, and 706 K. We measured thickness and crystal structure by the X-ray reflectivity(XRR) and X-ray

*E-mail: nagakubo@prec.eng.osaka-u.ac.jp

diffraction (XRD) methods with Co-Kα X-ray, respectively.

2.2 Picosecond ultrasound spectroscopy

To measure the elastic constant of the films, we use picosecond ultrasound spectroscopy, which uses ultrafast laser pulses to excite and detect GHz–THz ultrasound. We use a Ti-sapphire pulse laser whose wavelength and repetition rate are 800 nm and 80 MHz, respectively. We divide the pulse light into 15–40 mW pump and 4–6 mW probe light by a polarization beam splitter. The corner reflector changes the arrival time of the pump light to the specimen. The pump light is modulated at 100 kHz by an acousto-optical crystal modulator. The probe light wavelength is converted into 400 nm by a second harmonic generator. Both lights incident perpendicularly on the specimen through a 50-magnification objective lens, and the reflected lights are distinguished by a dichroic mirror, which reflects the 800-nm pump light and transmits the 400 nm-probe light. The beam splitter separates the probe light before incidence on the sample, and a balance detector collects these two lights. By inputting the intensity difference into a lock-in amplifier, we detect the probe light's reflectivity changes due to the acoustic perturbations.

3. Results and discussion

3.1 Efficiency function

We consider that Pt has an optimal thickness in the Pt/NiO/Pt structure: Thinner Pt makes the resonance frequency insensitive to the elastic constant of Pt. To quantitatively evaluate this effect, we define the contribution β_m of an elastic constant C_m to the resonance frequency f as follows:

$$\beta_m = \left| 2 \frac{\partial f}{\partial C_m} \frac{C_m}{f} \right| \tag{1}$$

This contribution is normalized to take a value between 0 and 1, and its summation for each layer becomes 1. Thinner Pt increases β_{NiO} and decreases β_{Pt}. However, it is difficult to excite and detect the resonance for a thinner Pt film because of two reasons. First, the energy of pump light pulse absorbed in Pt is decreased, decreasing the resultant phonon energy. Second, because of the zero-strain requirement at the free surface, the strain of very thin Pt layer is nearly zero, making the phonon detection through optoelastic interaction difficult. Therefore, we propose an efficiency function E_f as follows:

$$E_f(d_{\mathrm{Pt}}) = \beta_{\mathrm{NiO}} \int_0^{2d_{\mathrm{Pt}}} e^{-\alpha_{800} z} dz \times \int_0^{2d_{\mathrm{Pt}}} \overline{\varepsilon_{\mathrm{Pt}}}(z) e^{-\alpha_{400} z} dz, \tag{2}$$

where α_{800} and α_{400} are the absorption coefficients of the pump and probe light, respectively. Note that, $\alpha = 4\pi\kappa/\lambda$, where κ is the extinction coefficient of Pt for the light of wavelength λ. $\overline{\varepsilon_{\mathrm{Pt}}}$ is the normalized strain in the Pt layer, and d_{Pt} is the thickness of the single Pt layer. In this study, we fix the thicknesses of two Pt layers are the same. The first and second integral correspond to the absorbed light energy and detection efficiency of the probe light, respectively. Using a one-dimensional free-resonance model,[31–33] we calculate f and corresponding distributions of strain $\varepsilon_{\mathrm{Pt}}(z)$ and strain-energy $E(z)$ by solving an eigenvalue problem. To compare the amplitude of strain for different d_{Pt} structures, we normalize $\varepsilon_{\mathrm{Pt}}$ to make the integrated strain energy unity, obtaining $\overline{\varepsilon_{\mathrm{Pt}}}$.

Fig. 1(a) shows the calculated efficiency functions of the first and second modes for the NiO thickness d_{NiO} = 34 nm. The inset separately shows contributions and excitation-detection efficiency (the product of the two integral terms in eq. (2)). As Pt thickness increases, absorbed light and strain in Pt layer increase, leading to the increase in E_f until d_{Pt} ~20 nm. However, surface strain and the contribution decrease above it and absorbed light saturates, resulting in the peak in E_f around 15–20 nm.

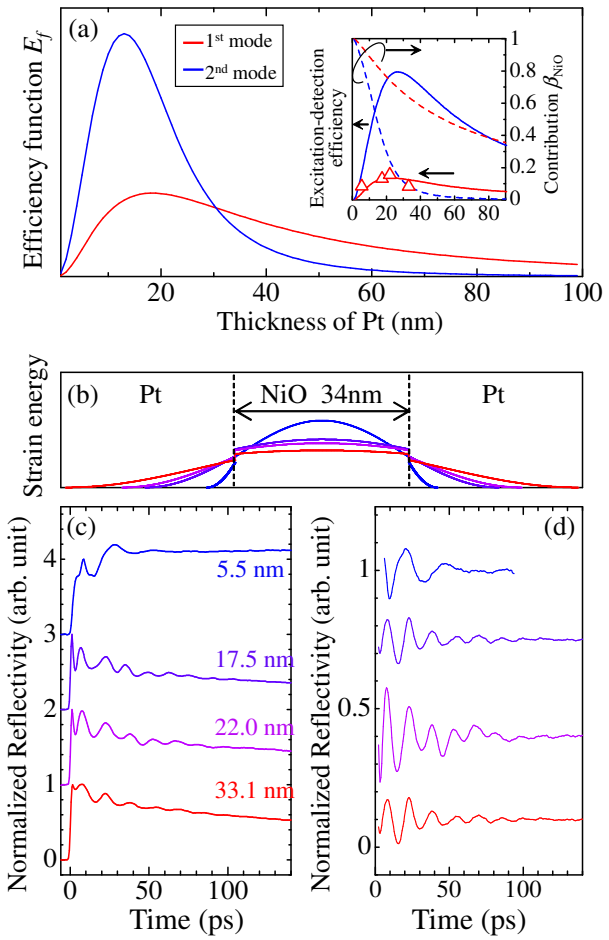

Fig. 1. (a) Calculated efficiency function E_f for d_{NiO} = 34 nm. Solid and dotted lines in inset represent excitation-detection efficiency and contribution β_{NiO} of the elastic constant of NiO to the resonance frequencies, respectively. Triangle plots in the inset represent measured resonance amplitudes of Pt/NiO/Pt films. (b) Calculated strain-energy distributions for d_{Pt} = 5.5, 17.5, 22.9, and 33.1 nm. (c) Observed reflectivity changes of Pt/NiO/Pt films deposited on AO substrate at room temperature, whose intensity is normalized at initial absorption intensity, and (d) extracted resonances.

To verify this function, we prepare four Pt/NiO/Pt films and measure the resonance amplitude by changing only d_{Pt} between 5.5 and 33.1 nm. Fig. 1(b) shows calculated strain-energy distributions of the fundamental mode. Observed reflectivity changes are shown in Fig. 1(c), whose amplitudes are normalized by the intensity at initial absorption. We extract the resonance by subtracting the background change due to thermal diffusion using a polynomial function as shown in Fig. 1(d). The strain energy of 5.5-nm film concentrates in the NiO layer, leading to high β_{NiO}. However, it is difficult to excite and detect its resonance as shown in Fig. 1(c) and (d).

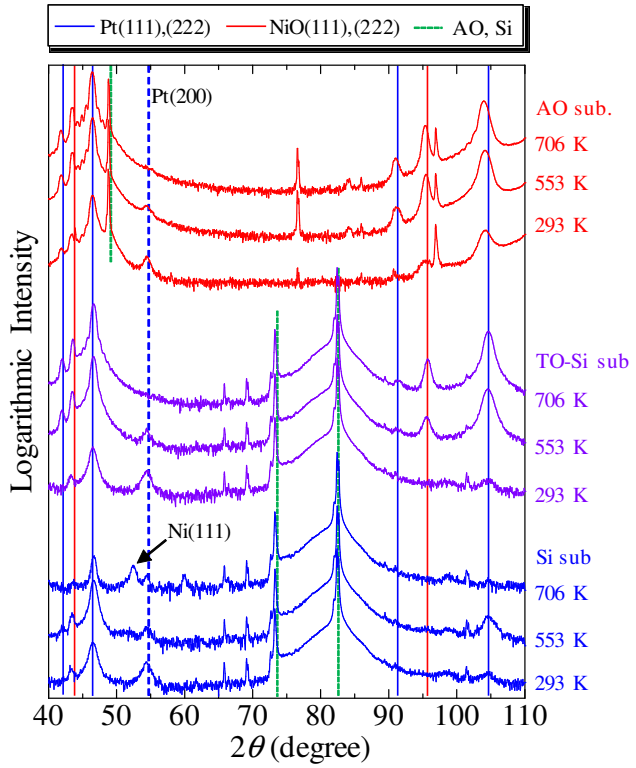

Fig. 2. XRD spectra of Pt/NiO/Pt films deposited on AO, TO-Si, and Si substrates.

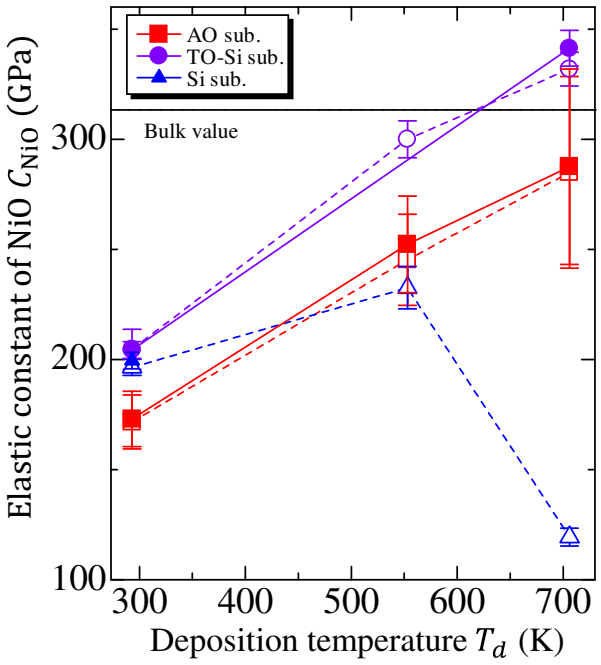

Fig. 3. Determined longitudinal elastic constant C_{NiO}. Closed symbols with solid lines and open symbols with dashed lines denote that we use the elastic constant of Pt of corresponding single-layer films and bulk values in the inverse calculation, respectively.

17.5-nm and 22.0-nm films show clear resonances, and the resonance amplitude decreases in the 33.1-nm film. We integrate the resonance amplitudes and compare the values with our model. Because we only evaluate the vibration amplitude in this measurement, we show the measured amplitudes in the inset in Fig. 1(a). They agree with the calculated excitation-detection efficiency, insisting on the validity of our model and E_f. Thus, we conclude that the optimal Pt thickness is ~18 nm for d_{NiO} = 34 nm.

3.2 Measure the elastic constant of NiO

To measure C_{NiO}, we make Pt/NiO/Pt films and Pt mono layers on AO, Si, and TO-Si substrates by changing deposition temperature T_d between 300 and 700 K. We measure d_{NiO} and d_{Pt} by the XRR method as listed in Table I (XRR spectra are shown in Fig. S1 in the supplementary material). XRD spectra shown in Fig. 2 reveal that increase in T_d enhances the crystallinity except T_d = 706 K for Si substrate: At T_d = 293 K, Pt shows (111) and (200) peaks, being polycrystalline. As T_d increases, the intensities of Pt (111) and NiO (111) increase, and the Pt-(200) peak disappears. Interface roughness also decreases (Table S1). However, the intensities of Pt peaks become weak in the film deposited on Si substrate at T_d = 706 K, and the film shows no NiO peaks and exhibits a Ni (111) peak, insisting that the crystal structure is deteriorated and NiO decomposes.

We observe the fundamental mode for all films and the second mode for the films deposited at T_d = 293 K (Fig. S2). We measure the resonance frequencies at 4–9 different points for each film, and inversely determine C_{NiO} by minimizing $\sum_i \left(1 - f_i^c / f_i^m\right)^2$, where f_i^c and f_i^m are calculated and measured resonance frequency of i-th mode. To calculate f_i^c, we need the value of C_{Pt}, and we measure it for the Pt mono layers deposited under the same condition as listed in Table I. We measure the thickness of them by the XRR method (Table S2 and Fig. S3(a)) and observe ~130 GHz resonance (Fig. S3(b-d)). We also use a C_{Pt} of bulk value[34] along <111> direction to determine C^*_{NiO}. We use the bulk values for mass density because calculated XRR spectra with bulk density well agree with measured spectra.

Determined C_{NiO} and C^*_{NiO} are shown in Fig. 3 and Table I. They agree with each other within 3% deviation, which is smaller than ~7% measurement deviations. C_{NiO} at T_d = 293 K is smaller than a corresponding bulk value[35] by ~ 40%, and it increases with T_d, approaches to the bulk value except for the Si substrate. Thin film contains many defects, and annealing treatment decreases defects at grain boundaries, resulting in the recovery of elastic constants.[36,37] However, on the Si substrate, the increase in T_d decomposes the crystal structure, decreasing the elastic constant. C_{NiO} of the films on AO substrate is smaller than that on TO-Si by ~16% at each temperature, and we consider that difference in crystallinity and interference structure due to substrates causes this softening.

3.3 Effects of other film parameters

To evaluate the determination error due to uncertainty of C_{Pt} and film thickness, we calculate resonance frequencies of first and second modes using bulk values, and inversely determined C_{NiO} from them by changing C_{Pt}, d_{Pt}, or d_{NiO} within ±10% in the inverse calculation. The deviations δC_{NiO} from the initial value are shown in Fig. 4. C_{Pt} of the three-layer structure might be different from that of mono layer even if they are deposited under the same condition. C_{Pt} of mono layer also contains measurement deviations. However, 5% changes of C_{Pt}, for example, causes ~3% deviations in C_{NiO}, which is smaller

Table I. Measured film thicknesses of Pt (d_{Pt}) and NiO (d_{NiO}) of Pt/NiO/Pt films, and longitudinal elastic constant of Pt (C_{Pt}) of mono-layer films at each deposition temperature T_d. C_{NiO} and C^*_{NiO} are the inversely determined elastic constant of NiO using C_{Pt} of the mono-layer films and a bulk, respectively. The standard deviations of C^*_{NiO} are equivalent to those of C_{NiO}.

Substrate	T_d (K)	d_{Pt} (nm)	d_{NiO} (nm)	C_{Pt} (GPa)	C_{NiO} (GPa)	C^*_{NiO} (GPa)
AO	293	17.52	34.42	369.9 ± 30.8	173.0 ± 12.5	171.6
	553	17.77	26.05	350.5 ± 14.0	252.3 ± 21.9	245.2
	706	17.94	27.24	374.3 ± 4.7	287.4 ± 44.4	284.8
TO-Si	293	17.97	33.46	357.6 ± 8.5	204.3 ± 3.8	204.6
	553	17.44	28.36			300.0
	706	17.97	28.37	357.4 ± 2.8	341.3 ± 8.2	331.8
Si	293	17.67	33.70	368.4 ± 0.0	199.0 ± 3.7	196.4
	553	17.11	26.18			232.6
	706					119.4

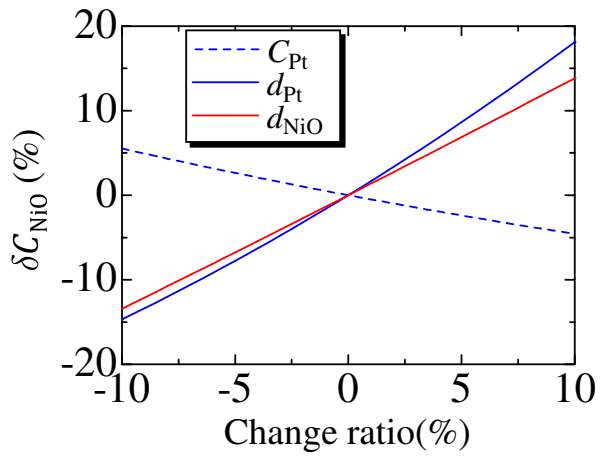

Fig. 4. Evaluated determination error δC_{NiO} in the elastic constant of NiO due to the changes of elastic constant of Pt (dashed line), film thicknesses of Pt and NiO (solid lines).

than typical measurement deviations of ~5%. On the other hand, 5% changes of film thickness causes ~8% deviations in C_{NiO}. Therefore, uncertainty of C_{Pt} less affects C_{NiO} in this structure. We measure film thicknesses by the XRR method, where measurement uncertainty is ~1% at most, leading to 2% deviations in C_{NiO}. Therefore, we conclude that this three-layer resonance method enables us to measure the elastic constant of ~30 nm dielectric film within measurement deviations.

4. Conclusions

To measure the longitudinal elastic constant of ~30 nm dielectric film, we use a three-layer structure. We propose an efficiency function to estimate the optimal thickness to determine the elastic constant of the dielectric film by considering its contribution to the resonance frequency and excitation-detection efficiency. We prepare four films by changing Pt-layer thickness as 5.5, 17.5, 22.0, and 33.1 nm, and measure their resonance amplitudes. Both of calculated efficiency and measured amplitudes have a peak around 20 nm, insisting the validity of our model. We conclude that the optimal Pt thickness is 18 nm for Pt/NiO/Pt structure for 34-nm NiO. We deposit the optimal-thickness Pt/NiO/Pt films by changing deposition temperatures between 300 and 700 K. We measure the resonance frequencies by picosecond ultrasonics, and inversely determine the elastic constant of NiO. The films deposited at room temperature has ~40% smaller elastic constant than a bulk. However, as the deposition temperature increases, crystallinity becomes better and the elastic constant approaches to the bulk value. We evaluate determination error of the elastic constant of NiO in this method, revealing that uncertainty of the elastic constant of Pt is smaller than measurement deviations and film thickness is more sensitive. We measure film thicknesses by the X-ray reflection method within ~1% uncertainty, leading to 2% deviations in the elastic constant of NiO. We conclude that this method enables us to measure the elastic constant of ~30 nm dielectric film within measurement deviations.

Acknowledgment

This work was supported by KAKENHI Grant No. 18H01859 of Grant-in-Aid for Scientific Research (B).

1) M. Kadota, T. Ogami, K. Yamamoto, Y. Negoro, and H. Tochishita, Jpn. J. Appl. Phys. **48**, 07GG08 (2009).
2) M. Kadota and T. Ogami, Jpn. J. Appl. Phys. **50**, 07HD11 (2011).
3) R. Goto, J. Fujiwara, H. Nakamura, and K. Hashimoto, Jpn. J. Appl. Phys. **57**, 07LD20 (2018).
4) M. Kadota, Y. Ishii, and S. Tanaka, Jpn. J. Appl. Phys. **59**, 07HD11 (2020).
5) M. Ueda, M. Hara, S. Taniguchi, T. Yokoyama, T. Nishihara, K. Hashimoto, and Y. Satoh, Jpn. J. Appl. Phys. **47**, 4007 (2008).
6) F. Thalmayr, K. Hashimoto, M. Ueda, T. Omori, and M. Yamaguchi, Jpn. J. Appl. Phys. **49**, 07HD11 (2010).
7) M. Hara, T. Yokoyama, T. Sakashita, S. Taniguchi, M. Iwaki, T. Nishihara, M. Ueda, and Y. Satoh, Jpn. J. Appl. Phys. **49**, 07HD13 (2010).
8) H. Kanbara, H. Kobayashi, and K. Nakamura, Jpn. J. Appl. Phys. **39**, 3049 (2000).
9) T. Kimura, K. Daimon, T. Ogami, and M. Kadota, Jpn. J. Appl. Phys. **52**, 07HD03 (2013).
10) T. Kimura, Y. Kishimoto, M. Omura, and K. Hashimoto, Jpn. J. Appl. Phys. **57**, 07LD15 (2018).
11) K. Matsumoto, M. Kadota , and S. Tanaka, Jpn. J. Appl. Phys. **59**, 036506 (2020).
12) H. Fukuda, A. Nagakubo, and H. Ogi, Proc. 41st Symp. Ultrasonic Electronics **41**, 3Pa1-3 (2020).
13) C. Thomsen, J. Strait, Z. Vardeny, H. J. Maris, J. Tauc, and J. J. Hauser, Phys. Rev. Lett. **53**, 989 (1984).
14) C. Thomsen, H. T. Grahn, H. J. Maris, and J. Tauc, Phys. Rev. B **34**, 4129 (1986).
15) H. Ogi, M. Fujii, N. Nakamura, T. Yasui, and M. Hirao, Phys. Rev. Lett. **98**, 195503 (2007).

16) N. Nakamura, H. Ogi, T. Yasui, M. Fujii, and M. Hirao, Phys. Rev. Lett. **99**, 035502 (2007).
17) A. Nagakubo, H. T. Lee, H. Ogi, T. Moriyama, and T. Ono, Appl. Phys. Lett. **116**, 021901 (2020).
18) H. Nakahata, H. Kitabayashi, T. Uemura, A. Hachigo, K. Higaki, S. Fujii, Y. Seki, K. Yoshida, and S. Shikata, Jpn. J. Appl. Phys. **37**, 2918 (1998).
19) K. Yamanouchi and T. Ishii, Jpn. J. Appl. Phys. **41**, 3480 (2002).
20) H. J. McSkimin, J. Appl. Phys. **24**, 988 (1953).
21) O. L. Anderson and H. E. Bömmel, J. Am. Ceram. Soc. **38**, 125 (1955).
22) C. D. Corso, A. Dickherber, and W. D. Hunt, J. Appl. Phys. **101**, 054514 (2007).
23) I. Koné, F. Domingue, A. Reinhardt, H. Jacquinot, M. Borel, M. Gorisse, G. Parat, F. Casset, D. Pellissier-Tanon, J. F. Carpentier, L. Buchaillot, and B. Dubus, Appl. Phys. Lett. **96**, 223504 (2010).
24) T. C. Zhu, H. J. Maris, and J. Tauc, Phys. Rev. B **44**, 4281 (1991).
25) H. Ogi, T. Shagawa, N. Nakamura, M. Hirao, H. Odaka, and N. Kihara, Phys. Rev. B **78**, 134204 (2008).
26) A. Nagakubo, H. Ogi, H. Ishida, M. Hirao, T. Yokoyama, and T. Nishihara, J. Appl. Phys. **118**, 014307 (2015).
27) A. Nagakubo, S. Tsuboi, Y. Kabe, S. Matsuda, A. Koreeda, and Y. Fujii, Appl. Phys. Lett. **114**, 251905 (2019).
28) A. Nagakubo, M. Arita, T. Yokoyama, S. Matsuda, M. Ueda, H. Ogi, and M. Hirao, Jpn. J. Appl. Phys. **54**, 07HD01 (2015).
29) A. Devos and R. Côte, Phys. Rev. B **70**, 125208 (2004).
30) A. Nagakubo, H. Ogi, H. Sumiya, K. Kusakabe, and M. Hirao, Appl. Phys. Lett. **102**, 241909 (2013).
31) H. Ogi, Y. Fukunishi, T. Omori, K. Hatanaka, M. Hirao, M. Nishiyama, and, Anal. Chem. **80**, 5494 (2008).
32) K. Uehara, H. Ogi, and M. Hirao, Appl. Phys. Express **7**, 025201 (2014).
33) A. Nagakubo, K. Adachi, T. Nishihara, and H. Ogi, Appl. Phys. Express **13**, 016504 (2020).
34) R. E. Macfarlane, J. A. Rayne, and C. K. Jones, Phys. Lett. **18**, 91 (1965).
35) N. Uchida and S. Saito, J. Acoust. Soc. Am. **51**, 1602 (1972).
36) N. Nakamura, H. Ogi, T. Shagawa, and M. Hirao, Appl. Phys. Lett. **92**, 141901 (2008).
37) N. Nakamura, Y. Nakamichi, H. Ogi, M. Hirao, and M. Nishiyama, Jpn. J. Appl. Phys. **52**, 07HB05 (2013).